Lifetime behaviour of unidirectionally wire reinforced lightweight metal matrix composites

Matthias Merzkirch, Volker Schulze, Kay A. Weidenmann

Angaben zur Veröffentlichung / Publication details:

Merzkirch, Matthias, Volker Schulze, and Kay A. Weidenmann. 2013. "Lifetime behaviour of unidirectionally wire reinforced lightweight metal matrix composites." *International Journal of Fatigue* 56: 60–68. https://doi.org/10.1016/j.ijfatigue.2013.08.002.

Lifetime behaviour of unidirectionally wire reinforced lightweight metal matrix composites

Matthias Merzkirch *, Volker Schulze, Kay André Weidenmann

Institute for Applied Materials (IAM–WK), Karlsruhe Institute of Technology (KIT), Engelbert-Arnold-Strasse 4, 76128 Karlsruhe, Germany

1. Introduction

The composite extrusion process [1] allows for a direct embedding of metallic and hybrid wires based on ceramic fibres [2,3] within lightweight metal matrices such as aluminium and magnesium alloys with the help of modified porthole dies. Until now a multitude of different continuous wire reinforced material combinations and profile geometries with an actual maximum reinforcing ratio of 13.5 vol.% could be produced [4].

First models about the quasi-static elastic tensile behaviour in longitudinal direction of unidirectionally reinforced composites have been expressed by [5,6]. The iso-strain model of Voigt [5] describes the strain of the composite (index C) which is equal to the strain within the reinforcing element (index RE) and the strain within the matrix (index M):

$$\varepsilon_C = \varepsilon_{RE} = \varepsilon_M \tag{1}$$

Furthermore the stress based rule of mixture [5,6] is deduced from the equilibrium of forces with respect to the volume ratio V of the reinforcing element and the matrix:

$$\sigma_C = \sigma_{RE} \cdot V_{RE} + \sigma_M \cdot V_M \tag{2}$$

With the help of Hooke's law the expression can be modified to the rule of mixture for the Young's modulus in longitudinal direction [5,6]:

$$E_C = E_{RE} \cdot V_{RE} + E_M \cdot V_M \tag{3}$$

The cyclic deformation behaviour of AZ31 under stress controlled fatigue testing has already been investigated by [7,8].

In [9] an overview of the investigations about the damage mechanisms of multiple continuous fibre reinforced MMCs is given. The damage behaviour of different unidirectionally metallic wire reinforced aluminium matrices under cyclic stress controlled loading has been studied in [10–12]. The reinforcing element leads to a significant increase in lifetime, noticeable by a parallel shift of the regression lines of the *S–N* curves in double logarithmic scale. In [10,12] metallographic investigations proved that crack initiation starts from the outer surface of 11.1 vol.% spring steel wire reinforced EN AW-60xx specimens continuing to grow until the crack reaches the reinforcing element. The crack growth of metallic rope reinforced EN AW-6060 [10] and wire reinforced EN AW-2099 [11] started from the interface between matrix and reinforcing element. A detailed view on damage behaviour of spring steel wire reinforced EN AW-6082 accompanied by the acoustic emission analysis has already been given in [12,13]. Altogether four stages of deformation and damage could be attested. After the hardening of the matrix material in stage I, stage II represents the saturation stage. Within stage III the crack initiates from the specimen's outer surface. By reaching the reinforcing element, beside the crack growth within the matrix material an additional debonding along the interface between the wire and the matrix could be confirmed. After the matrix fails at the end of stage III, the reinforcing element starts to fatigue with an initial hardening in stage IV until its complete failure [12,13].

* Corresponding author. Tel.: +49 721 608 42753; fax: +49 721 608 48044.
E-mail address: Matthias.Merzkirch@kit.edu (M. Merzkirch).

Advanced investigations about the bridging effect [14] of fibres during repeated loading in pure tension of unidirectionally reinforced MMCs with a broken matrix using the cyclic traction law (relationship between the fibre stress σ_{RE} and the pull-out displacement δ) have been made by [14–16]. After a first opening δ' the closure during unloading can be expressed by:

$$\Delta\delta'' = -\frac{d \cdot E_M \cdot (1 - V_{RE}) \cdot (\sigma_{RE,\max} - \sigma_{RE})^2}{(8 \cdot E_C \cdot E_{RE} \cdot \sigma_{deb} \cdot V_{RE}^2)} \quad (4)$$

And the following reopening can be expressed by:

$$\Delta\delta''' = \frac{d \cdot E_M \cdot (1 - V_{RE}) \cdot (\sigma_{RE} - \sigma_{RE,\min})^2}{8 \cdot E_C \cdot E_{RE} \cdot \sigma_{deb} \cdot V_{RE}^2} \quad (5)$$

where d represents the diameter of the reinforcing element and σ_{deb} the debonding shear strength of the interface.

A few attempts of a simple lifetime prediction of metal matrix composites have been done [17]. In [18]a model for a short-fibre reinforced aluminium alloy under strain controlled fatigue testing on basis of fracture mechanics has been introduced. An easier model in order to estimate the endurance limit deduced from multiple step tests for different wire reinforced EN AW-6060 matrices has been presented in [10] whereas the application was limited to a few wire reinforced material systems.

In [19,20] three different regimes of fatigue of MMCs have been distinguished which are dependent on the stress or strain range. For high ranges (regime 1) the damage is fibre failure dominated whereas regime 2 is matrix damage dominated (similar to monolithic metals). Low strain or stress ranges (regime 3) is threshold fatigue crack growth controlled. In [19] it has been assumed that the strain range (under strain as well as stress controlled testing) controls fatigue life within regime 2.

Since a simple prediction of lifetime of unidirectionally reinforced MMCs is missing, the aim of the current work is the derivation of a universal lifetime model out of the strain response, based on the understanding of mechanisms and mechanics of constituent deformation and damage evolution.

2. Material

The 40 × 10 mm^2 rectangular profiles were manufactured on a 10 MN extrusion press at the Institute of Forming Technology and Lightweight Construction at the TU Dortmund University. The matrix material is the magnesium alloy AZ31 (MgAl3Zn1), the reinforcing element is a spring steel wire (301SS) with a diameter of 1 mm.

The measured chemical composition of the matrix material is shown in Table 1 whereas aluminium and zinc lead to the hardening of the alloy.

The composition of the reinforcing element out of stainless spring steel is given in Table 2.

The composite profiles were made from the same matrix material and additionally reinforced during composite extrusion with four spring steel wires. Consequently, the reinforcing ratio is about 0.79 vol.%. Prior to the composite extrusion process the matrix material was heated up to a temperature of 360 °C, the ram speed was held constant at 1 mm/s. The profile was cooled with ambient air after the extrusion process. The press ratio was 22:1.

Table 1
Measured chemical composition of matrix material AZ31 in wt.%.

Al	Zn	Mn	Si	Fe	Ni	Sn	Mg
2.480	0.99	0.384	0.02	0.013	0.012	0.127	Bal.

Table 2
Measured chemical composition of the reinforcing element 301SS in wt.%.

C	Si	Mn	P	S	Cr	Ni	Mo	N	Fe
0.074	0.52	0.93	0.034	0.002	18.2	8.3	0.43	0.043	Bal.

Fig. 1a shows a detail of a cross section of the 40 × 10 mm^2 profile, with the embedded wire and the horizontally placed longitudinal weld seam (arrows). The detail of the interface in Fig. 1b shows the bonding between the wire and the matrix whereas the gap (dark area) between wire and matrix results from the metallographic etching [21]. The grain size distribution is relatively inhomogeneous.

In Table 3 the quasi-static properties of the single components and the composite material are listed. The debonding shear strength has been quantified using the push-out test [22] to σ_{deb} = 43 MPa. It has to be noticed that the offset yield strength of the unreinforced material is smaller in compression than in tension and vice versa for the composite.

3. Specimen geometry and experimental procedure

All specimens have been tested in longitudinal (extrusion) direction. The specimen geometry for the fatigue tests is shown in Fig. 2. The gauge length of the cylindrical specimens was 10 mm with a diameter of 3 mm. The centrically placed wire (dashed line) had a diameter of 1 mm resulting in a volume ratio of V_{RE} = 11.1% in the gauge length. The specimen ends were face-turned for proper application of sensors for the acoustic emission analysis described in detail in [12,13].

The stress controlled fatigue tests were carried out in environmental atmosphere with an electro-dynamic testing machine Instron E3000 at a stress ratio of $R = -1$ (fully reversed loading) and a sinusoidal loading frequency of 10 Hz. The strain was measured with a capacitive measuring gauge attached to the specimen. Three specimens have been tested per load level and the maximum of the number of cycles till test end (run out) was chosen to be 10^7 cycles.

4. Results

4.1. Lifetime behaviour

Fig. 3 shows the S/N curves in double logarithmic scale for the unreinforced and the 11.1 vol.% spring steel wire reinforced AZ31. The values shown are average values derived from three tests per stress level. The regression lines have been interpolated between 110 MPa and 170 MPa for the unreinforced resp. between 110 MPa and 200 MPa for the 11.1 vol.% reinforced composite. Additionally, the extrapolated values from 0.25 up to 10^7 cycles and the quasi-static values for the 0.2% offset yield strength $R_{p0.2}$ as well as the ultimate tensile strength σ_{UTS} are given.

For the unreinforced material a sharp deflection of the curve can be attested between 120 MPa and 105 MPa, which tendency is visualised by the dotted line. By comparing the measured endurance

Table 3
Quasi-static properties of the single components and the composite material.

	E (GPa)	$R_{p0.2\ tens}$ (MPa)	$R_{p0.2\ comp}$ (MPa)	σ_{UTS} (MPa)
301SS	197	1963	–	2095
AZ31	42	198	124	289
AZ31 + 301SS (11.1 vol.%)	54	267	323	410

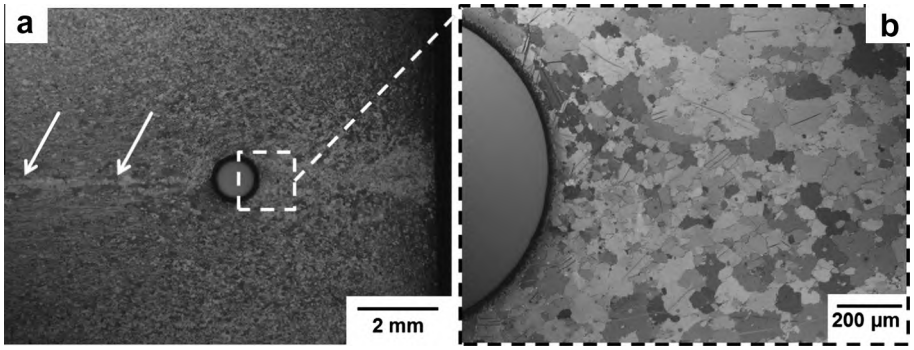

Fig. 1. Cross section of a 40 × 10 mm^2 profile: (a) overview and (b) detail of the interface.

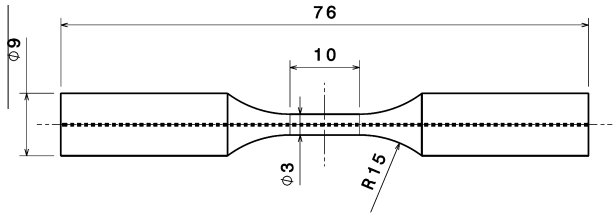

Fig. 2. Specimen geometry for the cyclic fatigue tests with dimensions in mm.

limit for the unreinforced and the reinforced material, no improvement can be deduced by the use of a reinforcing element.

It can be concluded that the reinforcement of 11.1 vol.% leads to an increase in lifetime in comparison to the unreinforced material which can be seen by a parallel shift of the regression lines.

Table 4 lists the measured and extrapolated endurance limit $S_{e/10\text{^}7}$ as well as the parameters for the unreinforced and the reinforced material under consideration of the Basquin relation [23] for the regression lines. There is a good agreement in the determined endurance limit with the mathematical regression and the fatigue-tested reinforced specimen without rupture.

The comparable exponent b explains the parallelism of the two regression lines shown in Fig. 3.

4.2. Deformation and damage behaviour

Generally three different stages of deformation and damage can be detected for the unreinforced material. Fig. 4a depicts representative hysteresis loops for the hardening stage I (second and 50th cycle) and for the saturation stage II (N/N_f = 50%). Due to the regulation of the testing machine, the set maximum stress cannot be reached within the first cycles which leads to a deviation in comparison to the default value (σ_a = 125 MPa). Comparison of the hysteresis loops of the second and the 50th cycle shows the shift to higher strains. This can be lead back to the pre-plastification in tension and the subsequent (smaller) plastification in compression. A pronounced asymmetric deformation behaviour during hardening, as it is shown in [7,8], is absent for the applied loading. Furthermore the cyclic hardening can be seen with the help of the narrowing of the hysteresis with increasing cycles.

Fig. 4b shows representative hysteresis loops for the damage stage III. Damage initiation is marked as a visible reduction of the unloading stiffness in tension after load reversal. Afterwards the hysteresis is shifted to higher total mean strain $\varepsilon_{t,m}$ due to crack growth. This leads furthermore to an increase of the strain in tension.

In contrast, the composite material shows four different stages of deformation and damage. Fig. 5 shows the hysteresis loops for stages I–II (a) and III (b). During the cyclic hardening (stage I), beside the narrowing hysteresis loops, an additional shift of the hysteresis loops to higher total strains can be observed until the saturation state is reached, Fig. 5a. A possible explanation can be found in pre-plastification in tension and the subsequent (smaller) plastification in compression or in the asymmetric deformation behaviour due to the strength-differential effect where hardening in tension starts at higher amount stresses than in compression (compare Table 3).

Within stage III, in addition to the broadening of the loops, the stress–strain response varies from nearly linear to a deflection of the curves. The tensile strain is larger than the compressive strain due to the increasing crack growth within the matrix material until its complete fracture at the end of stage III. For further investigations on the damage behaviour, the stiffness of unloading in tension S^{+}_{unl} and in compression S^{-}_{unl} has been visualised too.

Fig. 6 shows the hysteresis loops for stage IV during fatigue of the remaining reinforcing element after fracture of the matrix material. For the hysteresis of the matrix fracture ($N_{f,M}$) the slope indicating the stiffness during loading in compression S^{-}_{unl} = 50 GPa shows that the crack is fully closed since the composites Young's modulus is

Table 4
Endurance limit S_e and Basquin parameters of the matrix material and the 11.1 vol.% composite.

	$S_{e/10\text{^}7}$ (MPa)	$S_{e/10\text{^}7\ \text{extrapolated}}$ (MPa)	σ'_B (MPa)	b
AZ31	100	73	337	−0.0945
AZ31 + 301SS (11.1 vol.%)	100	105	447	−0.0896

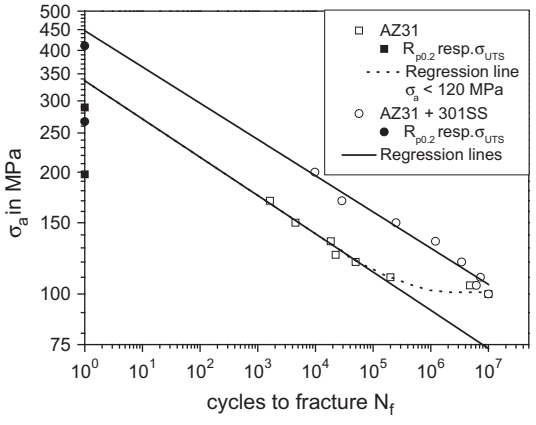

Fig. 3. S/N curves of the unreinforced and the 11.1 vol.% spring steel wire reinforced AZ31 composite material.

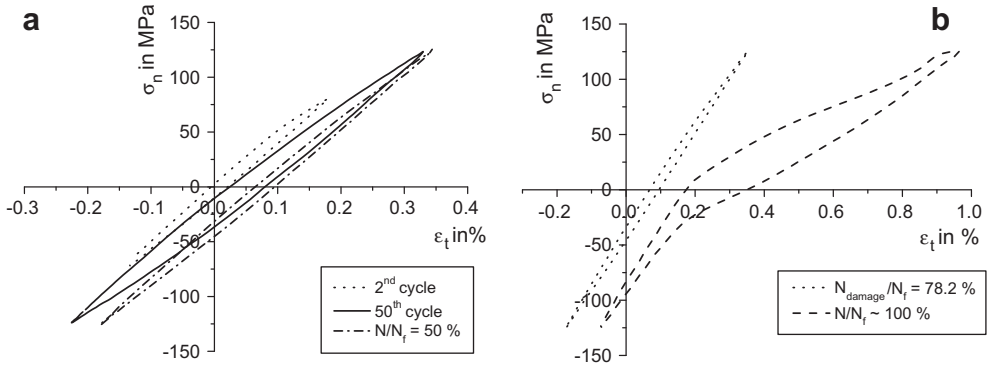

Fig. 4. Hysteresis loops for the matrix: (a) stage I–II and (b) stage III (σ_a = 125 MPa, N_f = 34,912).

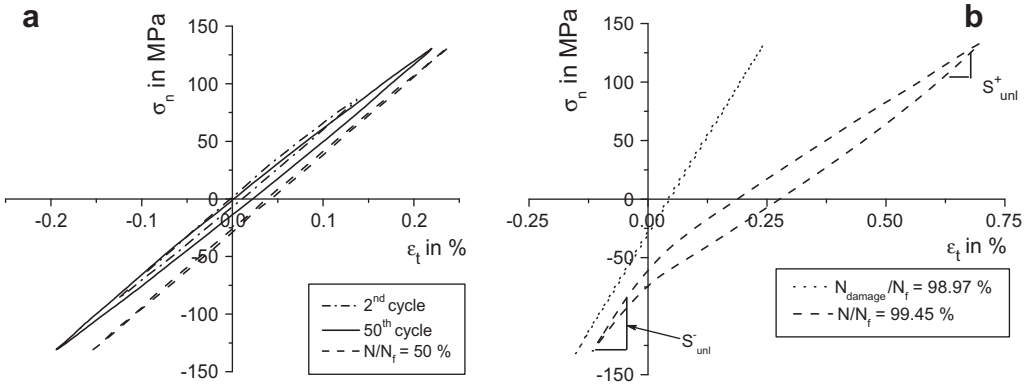

Fig. 5. Hysteresis loops for the composite: (a) stages I–II and (b) stage III (σ_a = 135 MPa, N_f = 1,195,290).

nearly reached (see Table 3). After fracture of the matrix material the hysteresis loops enlarge and a shift to higher strains can be noticed. Both hysteresis loops show a progressive increase during unloading in tension (see arrow).

The quantification of deformation and damage behaviour of the composite material with the help of the plastic strain amplitude $\varepsilon_{pl,a}$ against the relative number of cycles to fracture N/N_f is shown in Fig. 7. In order to describe the evolution of damage, a parameter D based on the loss in stiffness (increase of compliance) in tension [12,13,24,25] due to crack growth is shown in Fig. 7. D is defined by the following equation:

$$D[\%] = \frac{S^+_{unl(ave1-100)} - S^+_{unl(i)}}{S^+_{unl(ave1-100)}} \quad (6)$$

where S^+_{unl} characterises the unloading stiffness in tension, see Fig. 5b; the index i represents the current cycle and (ave1 – 100) the average value of the first 100 cycles as a reference.

Initially a decrease of the plastic strain amplitude $\varepsilon_{pl,a}$ for the composite material as well as for the unreinforced material (stage I) is observable. This can be described by the cyclic hardening of the matrix material due to the formation and interaction of twins for higher amplitudes and dislocation slipping is predominant at lower amplitudes [26–29]. Stage II represents the quasi-saturation state with almost constant plastic strain amplitude. Stage III describes the crack growth within the matrix material represented by the increase of the damage parameter D and the increase of the plastic strain amplitude $\varepsilon_{pl,a}$. It has to be noticed that the plastic strain amplitude is less sensitive to crack growth than the damage parameter D.

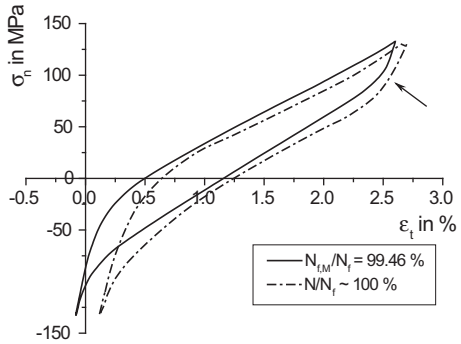

Fig. 6. Hysteresis loops for stage IV of the composite (σ_a = 135 MPa, N_f = 1,195,290).

At the end of stage III the matrix material is completely fractured. For the composite stage IV represents the fatigue of the reinforcing element, Fig. 7b.

Fig. 8 shows a zoom of stage IV, the fatigue of the reinforcing element. The hardening of the reinforcing element can be seen by an initial decrease of the plastic strain amplitude $\varepsilon_{pl,a}$. The end of stage IV is characterised by the fracture of the reinforcing element accompanied with the complete failure of the composite.

4.3. Metallographic and fractographic investigations

Fig. 9 shows the crack tips at the surface of an 11.1 vol.% reinforced specimen for stage III. The specimen with a diameter of 3.3 mm has been polished in several steps down to a diameter of 3 mm. After the increase of the mechanical damage parameter D,

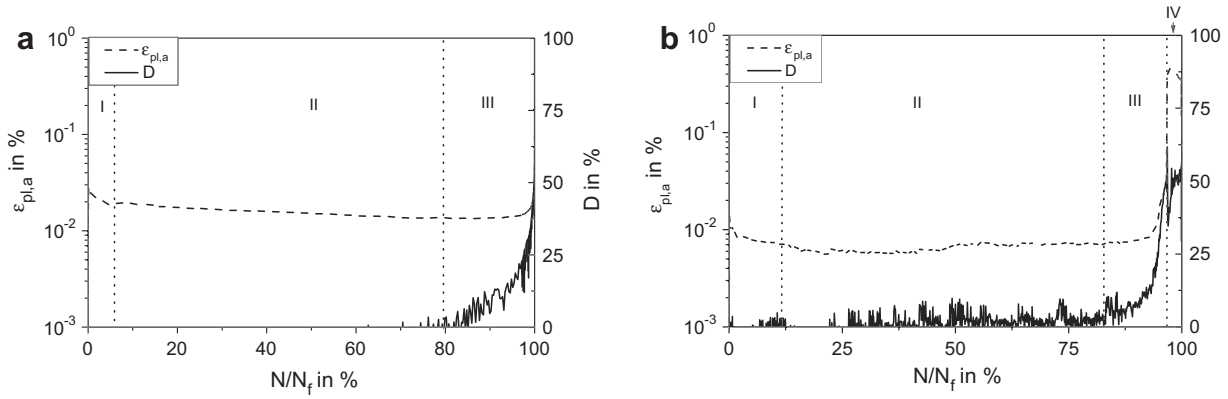

Fig. 7. Representative cyclic deformation curves for the unreinforced material ((a) σ_a = 125 MPa, N_f = 34,912) and for the composite ((b) σ_a = 135 MPa, N_f = 106,200).

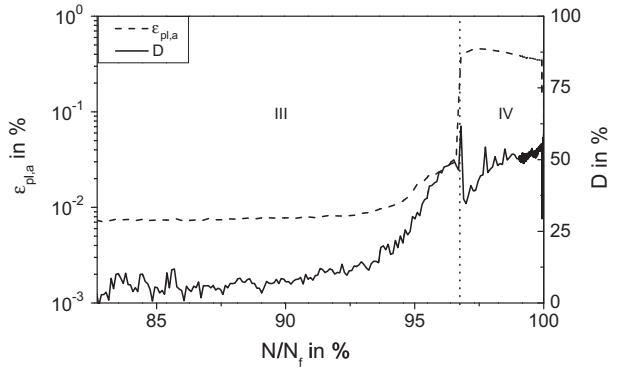

Fig. 8. Representative cyclic deformation curve (zoom in) of the composite (σ_a = 135 MPa, N_f = 106,200).

the test has been stopped and the specimen's surface has been observed metallographically. The loading direction is horizontal.

Fig. 9a and c show that beside the main crack, slip bands close to the crack can be observed (see arrows). The dashed line in Fig. 9a illustrates the plastic deformation (also in radial direction) which has been increased with further 80 cycles, Fig. 9b. Also the slip band density has increased. Comparing the crack length of Fig. 9c and d, a crack growth of about 340 µm can be observed.

Fig. 10a shows a longitudinal section of another loaded specimen (for stage III) to visualise the crack growth within the matrix material, outgoing from the outer specimen's surface. With increasing crack length, an additional debonding between matrix material and reinforcing element, a crack growth along the interface resp., can be observed, Fig. 10b.

Fig. 11a shows fractographic images of an 11.1 vol.% reinforced specimen. The details in Fig. 11b show the debonding around the reinforcing element (arrows). Furthermore the morphology of the fatigue crack growth can be observed. Regarding the remaining surface, the area of the overload fracture is larger than that of the fatigue crack growth within the reinforcing element (dashed white line).

It can be concluded that the crack initiation starts from the outer surface of the specimen within the matrix material. The crack growth continues within the matrix material until the crack reaches the reinforcing element. In addition to the crack growth around the reinforcing element, a crack growth along the interface between the matrix material and the reinforcing element (debonding) parallel to the loading direction can be observed. At the end of stage III the matrix is completely fractured and the fatigue of the reinforcing element within stage IV continues until the complete fracture of the composite.

5. Discussion

5.1. Fatigue of the reinforcing element

After fracture of the matrix (beginning of stage IV), Eqs. (4) and (5) can be used in order to describe the bridging effect of the exposed wire during continuous loading and unloading (via cyclic traction law). Fig. 12 shows the comparison of the hysteresis loop at matrix fracture ($N_{f,M}$) and the applied model. The strain ε_t resp. the crack opening δ is normalised so that 0 stands for full crack closure at a stress where the stiffness during unloading $\bar{S}_{unl}$ is equal to the composite stiffness, see Fig. 5b. Full crack opening is expressed by 1.

A relatively good agreement between the applied model and the measured hysteresis can be attested during loading, whereas the crack opening during unloading is overestimated. An explanation could be the interface degradation during continuous loading and unloading [16]. The reduction in sliding stress (interfacial strength) will reduce the shielding associated with bridging fibres [16]. It has to be noted that crack growth within the interface already starts during stage III (see Fig. 10), so that there is already advanced interface degradation compared to the initial state.

Since stage IV describes the fatigue of the reinforcing element, N_{IV} represents the cycles to fracture of the reinforcing element. Due to the fact that the loading ratio R within the reinforcing element cannot be clearly determined, see Fig. 6, the maximum stress within the reinforcing element $\sigma_{RE,max}$ is calculated via Eq. (2) with the stress amplitude σ_a neglecting the term of the matrix. Fig. 13 shows the S/N curves for the reinforcing element within the AZ31 matrix and the EN AW-6082 matrix [12].

The overlap of the two S/N curves for the different material systems verifies that the reinforcing element only fatigues in stage IV.

5.2. Lifetime model

Since a simple model for the prediction the lifetime of continuous fibre reinforced composites is missing, this section leads to the development of a new model out of the mechanical (quasi-static and cyclic) data of the single components based on the iso-strain model [5] (Eq. (1)) and the rules of mixture [5,6] (Eqs. (2) and (3)).

Similar to the investigations done by [19,20] where the strain range controls fatigue life, Fig. 14 shows the average values for the total strain amplitude $\varepsilon_{t,a}$ versus the cycles to fracture and the regression lines in double logarithmic scale for the unreinforced material and the 11.1 vol.% reinforced composite. The total

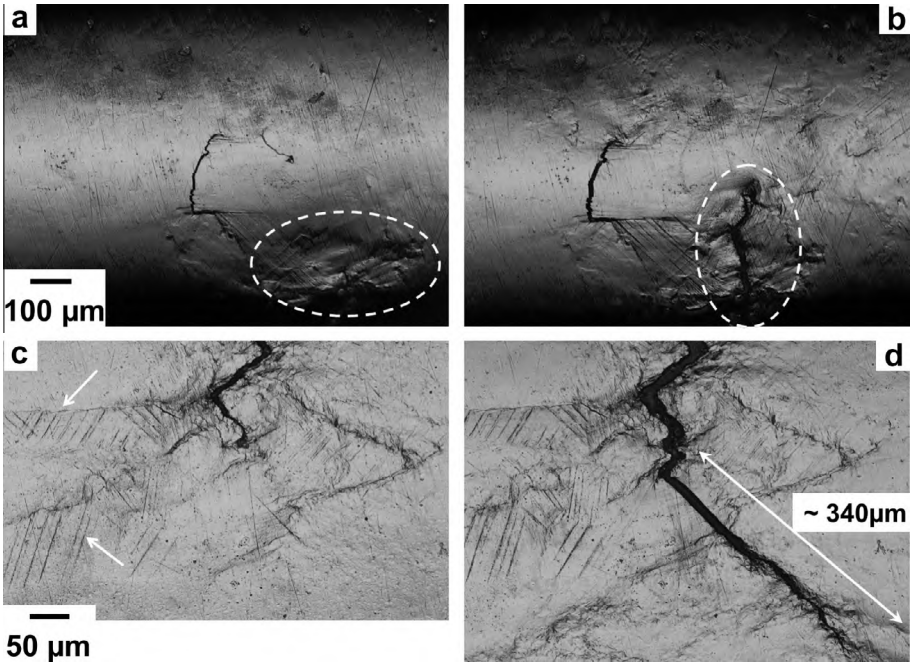

Fig. 9. Microscopic pictures of the surface of the crack tips: (a) and (b) top, (c) and (d) bottom: (a) and (c) N = 16,960 cycles, (b) and (d) 17,040 cycles (σ_a = 170 MPa).

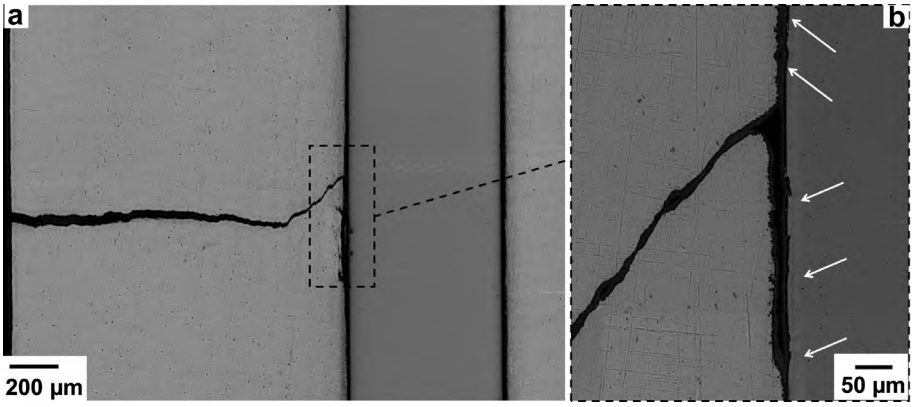

Fig. 10. Longitudinal sections: (a) overview and (b) zoom in of the interface (σ_a = 170 MPa, N = 17,040).

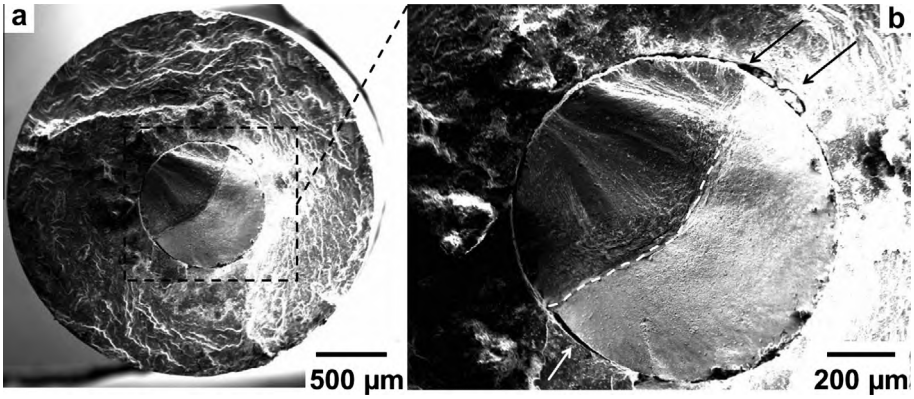

Fig. 11. SEM fractographic pictures of the composite: (a) overview and (b) zoom in (σ_a = 170 MPa, N = 17,040).

strain amplitudes have been derived from the strain response within the quasi-saturation state II (half lifetime $N_f/2$) from the stress controlled S/N curves.

It can be seen that the regression lines both for the unreinforced and the 11.1 vol.% reinforced composite are comparable. Consequently (in agreement to [19,20]) it can be concluded that

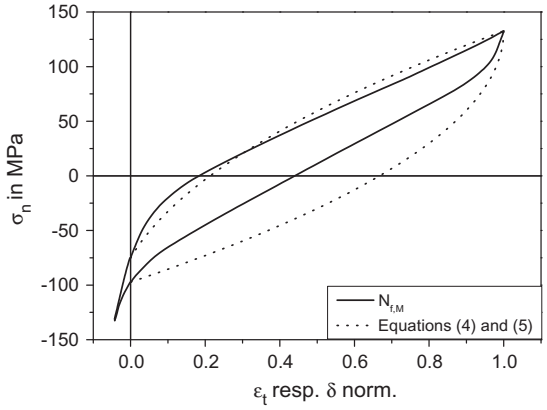

Fig. 12. Hysteresis loop at matrix fracture $N_{f,M}$ in comparison to the cyclic traction law (σ_a = 135 MPa, N_f = 1,195,290).

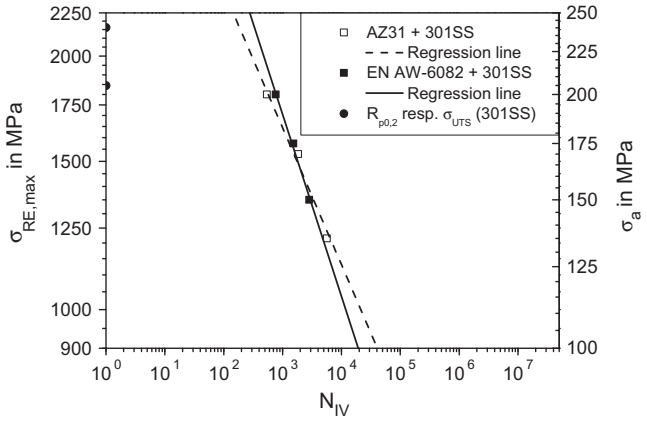

Fig. 13. *S*/*N* curves of the reinforcing element of the composite AZ31 + 301SS and EN AW-6082-T4 (F) + 301SS [12].

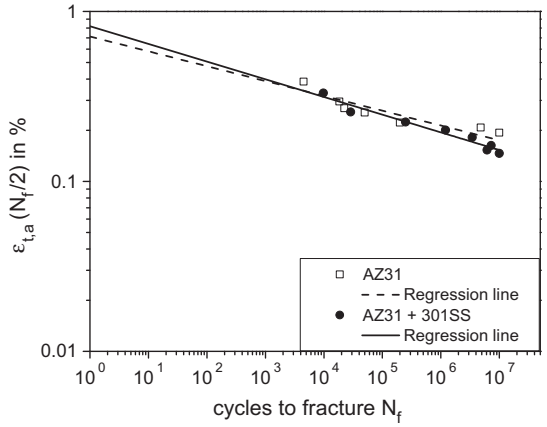

Fig. 14. Total strain amplitude $\varepsilon_{t,a}$ versus number of cycles to fracture N_f for the 11.1 vol.% reinforced composite and the unreinforced material.

the lifetime of the composite (C) is equal to the one of the unreinforced material (M) for the given total strain amplitudes which can be expressed by the following equation:

$$\varepsilon_{t,a}(\sigma_{a,C}) = \varepsilon_{t,a}(\sigma_{a,M}) \quad \text{if } N_f(C) = N_f(M) \tag{7}$$

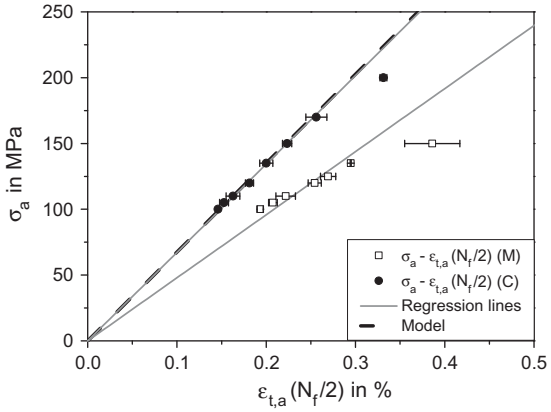

Fig. 15. Cyclic stress–strain curves for the 11.1 vol.% reinforced and the unreinforced material.

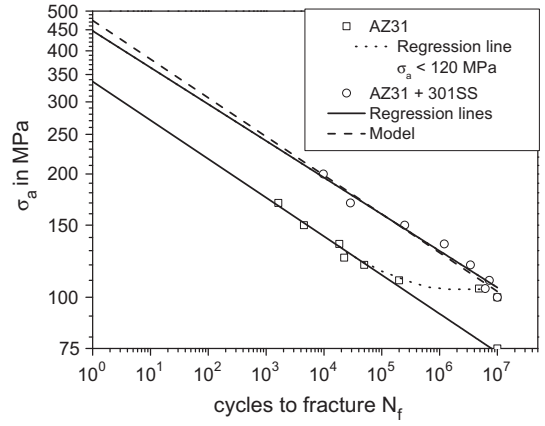

Fig. 16. *S*/*N* curves for the unreinforced material and comparison of the 11.1 vol.% reinforced composite to the applied model.

and is analogous to Eq. (1). In order to calculate the stress amplitude for the composite, assuming that the lifetime for the unreinforced is equal to the reinforced material at the same total strain amplitudes (see Eq. (1)), the following equation can be expressed with Hooke's law:

$$\frac{\sigma_C}{E_C} = \frac{\sigma_M}{E_M} \rightarrow \sigma_C = \sigma_M \cdot \frac{E_C}{E_M} \tag{8}$$

By using Eqs. (2) and (3), Eq. (8) can be transformed to:

$$\sigma_C = \sigma_M \cdot \left(\frac{E_C}{E_M} \cdot V_{RE} + (1 - V_{RE})\right) \tag{9}$$

Since the total strain amplitudes at half lifetime shown in Fig. 14 are measured at different stress amplitudes, Fig. 15 shows the relationship between stress amplitude σ_a and total strain amplitude $\varepsilon_{t,a}$ with the help of cyclic stress–strain curves of the reinforced and the unreinforced material.

Beside the regression lines for the unreinforced and the 11.1 vol.% reinforced composite, Eq. (9) (referred to as model) is shown. The good correlation between the regression lines (Young's modulus) of the unreinforced material and the composite verifies that the damage occurs within the last half of the lifetime. Furthermore there is a good agreement between the regression line of the composite and Eq. (9).

By using the Basquin relation [23] for the matrix material, Eq. (9) can be modified as:

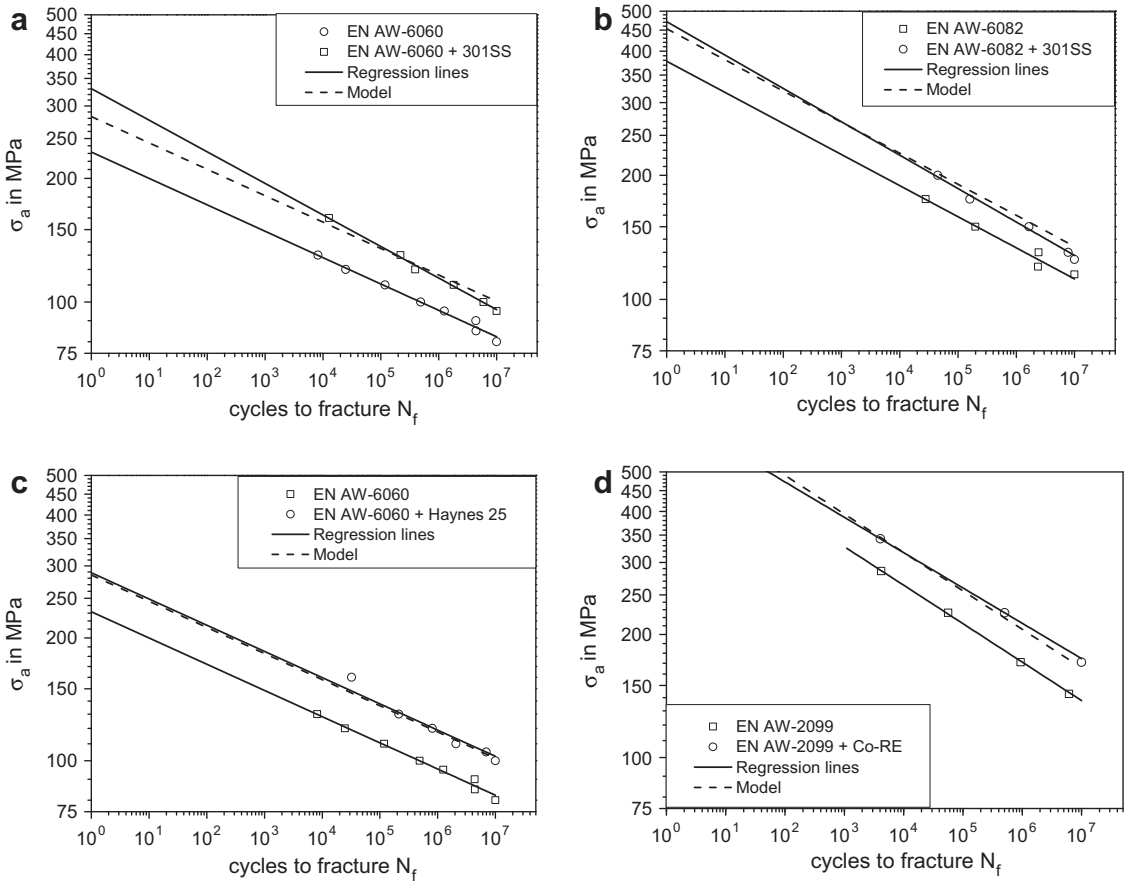

Fig. 17. Application of the model to different material systems: (a) EN AW-6060 + 301SS [10], (b) EN AW-6082 + 301SS [12], (c) EN AW-6060 + Haynes 25 [10], and (d) EN AW-2099 + Co-based RE [11].

$$\sigma_{a,C} = \sigma'_{B,M} \cdot (N_f(M))^b \cdot \left(\frac{E_C}{E_M} \cdot V_{RE} + (1 - V_{RE})\right) \tag{10}$$

Fig. 16 shows measured *S*/*N* curves of the unreinforced and reinforced material as well as the comparison with the applied model (Eq. (10)). A very good agreement between the applied model and the reinforced behaviour can be attested.

In order to check the applicability of the presented model to other material systems, it is assumed that the same deformation and damage behaviour occurs. The model has been used for material systems with different reinforcing elements (Haynes 25 and another cobalt based wire) and different hardenable aluminium matrix materials (EN AW-2099, EN AW-6060, EN AW-6082), Fig. 17. Other than for AZ31 + 301SS, it can be concluded that beside the estimation of lifetime of reinforced light weight metals, the model also provides a relatively good prediction of the endurance limit. It can be summarised that the derived model gives a good prediction of the lifetime for several unidirectionally reinforced metal matrix composites.

6. Conclusions

The present investigations have shown that an unidirectionally spring steel wire reinforced magnesium alloy AZ31 with a reinforcing ratio of 11.1 vol.% leads to significantly higher fatigue lifetimes in comparison to the single matrix material. The endurance limit was only hardly affected by the addition of a reinforcing element. In [30,31] investigations about the deflection of the *S*/*N* curves for AZ31 at lower stress amplitudes have been done. The reason for the deflection of the curve can be found in different crack initiation behaviour along the different phases of the alloy.

Altogether four stages of deformation and damage could be identified for the composite with the evolution of the plastic strain amplitude and a damage parameter *D* and qualified with metallographic analyses according to the investigations done in [12,13] on spring steel wire reinforced EN AW-6082. Starting with the hardening of the matrix material in stage I the quasi-saturation state II follows. Furthermore, it has already been shown in [10–13] that stage III represents the damage mechanisms such as crack initiation from the specimen's outer surface and growth within the matrix material followed by an additional debonding along the interface between wire and matrix. At the end of stage III the fracture of the matrix material occurs which is followed by the fatigue of the reinforcing element in stage IV. Due to crack growth in the reinforcing element and the continuing interface degradation it is assumed that the stress ratio *R* of the reinforcing element is changing with increasing cycles. According to [19] it can be concluded that the fatigue life of this composite under the applied stress ranges is matrix damage dominated.

The bridged matrix cracking (beginning of stage IV) could successfully be described during loading using the model by [14–16]. In [16] it has been deduced that the increasing deflection of the hysteresis loops could be lead back to advancing interface degradation. A consideration of the interface degradation with the help of the varying interfacial strength, as shown in [16], could optimise the crack opening during unloading.

Based on the investigations done in [19], out of the strain response of the stress controlled fatigue tests an innovative model for continuous fibre reinforced metal matrix composites could be

developed which allows for a very good estimation of fatigue lifetime. In comparison to other lifetime models [17,18] the great advantage of the presented model lies in the little data needed. With the help of the quasi-static values (Young's modulus) of the components, the reinforcing ratio and the knowledge of the fatigue behaviour of the single matrix material the application could be expanded to other material systems with different matrix materials and reinforcing elements which also showed a very good agreement to the experimental investigations. The condition for the application is a comparable damage behaviour as shown.

A further application for this lifetime model could be the variation of the reinforcing ratio as well the verification under different *R*-ratios.

Acknowledgments

This paper is based on investigations of the subproject A3 – "Material systems for reinforced and functional extruded profiles" – of the Collaborative Research Center/Transregio 10 which is kindly supported by the German Research Foundation (DFG). The authors would like to thank A. Henschel for contributing to the experiments.

References

[1] Kleiner M, Schomäcker M, Schikorra M, Klaus A. Manufacture of extruded and continuously reinforced aluminum profiles for ultra-lightweight constructions. Materialwiss Werkstofftech 2004;35(7):431–9.
[2] Weidenmann KA, Schomäcker M, Kerscher E, Löhe D, Kleiner M. Composite extrusion of aluminium matrix specimens reinforced with continuous ceramic fibres. Light Metal Age 2005;63(5):6–10.
[3] Merzkirch M, Weidenmann KA, Kerscher E, Löhe D, Pietzka D, Schikorra M, et al. Mechanical properties of hybrid composite extrusions of an aluminum-alumina wire reinforced aluminum alloy. Mater Sci Technol (MS&T) Pitt 2008:2552–62.
[4] Schomäcker M, Schikorra M, Kleiner M. 4 Years of research on composite extrusion for continuous reinforcement of aluminium profiles. In: 6th Aluminium two thousand world congress, Florence (Italy); 2007.
[5] Voigt W. Theoretische Studien über die Elasticitätsverhältnisse der Krystalle, Abh Kgl Ges Wiss Göttingen Math 1887;K134:3–51.
[6] Kelly A, Davies J. The Principles of the fibre reinforcement of metal. Metall Rev 1965;10(37):1–78.
[7] Jägg S, Zinn W, Scholtes B. The cyclic deformation behaviour of Mg-base alloy AZ31. Materialwiss Werkstofftech 1999;30:65–71.
[8] Morita S, Tanaka S, Ohno N, Kawakami Y, Enjoji T. Cyclic deformation and fatigue crack behavior of extruded AZ31B magnesium alloy. Mater Sci Forum 2010;638–642:3056–61.
[9] Schulte K, Minoshima K. Damage mechanisms under tensile and fatigue loading of continuous fibre-reinforced metal-matrix composites. Composites 1993;24(3):197–208.
[10] Weidenmann KA, Schwind Th, Kerscher E, Löhe D. Cyclic loading of wire-reinforced aluminium matrix composite extrusions. Materialwiss Werkstofftech 2007;38(2):75–8.
[11] Weidenmann KA, Kerscher E, Hammers T. Mechanical properties of compound extruded aircraft stringer profiles under cyclic loading. Adv Eng Mater 2010;12(1):584–6.
[12] Weidenmann KA, Kerscher E, Merzkirch M. In situ damage detection with acoustic emission analysis during cyclic loading of wire reinforced EN AW-6082. Adv Eng Mater 2010;12(1):637–40.
[13] Merzkirch M, Reeb A, Weidenmann KA, Wanner A, Schulze V. Acoustic response of reinforced lightweight metal matrix composites during tensile and cyclic loading. J Acoust Emission 2011;29:317–28.
[14] McMeeking RM, Evans AG. Matrix fatigue in fibre composites. Mech Mater 1990;9:217–27.
[15] Cox BN, Marshall DB. Crack bridging in the fatigue of fibrous composites. Fatigue Fract Eng Mater Struct 1991;14(8):847–61.
[16] Walls DP, Zok FW. Interfacial fatigue in a fiber reinforced metal matrix composite. Acta Metall Mater 1994;42(8):2675–81.
[17] Johnson WS, Larsen JM, Cox BN. ASTM Symposium on Life Prediction Methodology for Titanium Matrix Composites, STP 1253; 1996.
[18] Ding H-Z, Biermann H, Hartmann O. A low cycle fatigue model of a short-fibre reinforced 6061 aluminium alloy metal matrix composite. Compos Sci Technol A 2002;62:2189–99.
[19] Majumdar BS, Newaz GM. Constituent damage mechanisms in metal matrix composites fatigue loading, and their effects on fatigue life. Mater Sci Eng A 1995;200:114–29.
[20] Talreja R. A conceptual framework for interpretation of MMC fatigue. Mater Sci Eng A 1995;200:21–8.
[21] Kree V, Bohlen J, Letzig D, Kainer KU. The metallographical examination of magnesium alloys. Prakt Metallogr 2004;41(5):233–46.
[22] David Marshall B. An indentation method for measuring matrix-fibre frictional stresses in ceramic composites. Commun Am Ceram Soc (1984) C-259–C-260.
[23] Basquin OH. The exponential law of endurance tests. Proc ASTM 1910:625–30.
[24] Lemaitre J, Chaboche JL. Aspect phénoménologique de la rupture par endommagement. Journal de mécanique appliquée 1978;2(3):317–65.
[25] Biermann H, Vinogradov A, Hartmann O. Fatigue damage evolution in a particulate-reinforced metal matrix composite determined by acoustic emission and compliance method. Zeitschrift für Metallkunde 2002;93(7):719–23.
[26] Begum S, Chen DL, Xu S, Luo Alan A. Low cycle fatigue properties of an extruded AZ31 magnesium alloy. Int J Fatigue 2009;31:726–35.
[27] Matsuzuki M, Horibe S. Analysis of fatigue damage process in magnesium alloy AZ31. Mater Sci Eng A 2009;504:169–74.
[28] Yin SM, Yang HJ, Li SX, Wua SD, Yang F. Cyclic deformation behavior of as-extruded Mg–3%Al–1%Zn. Scripta Mater 2008;58:751–4.
[29] Koike J, Fujiyama N, Ando D, Sutou Y. Roles of deformation twinning and dislocation slip in the fatigue failure mechanism of AZ31 Mg alloys. Scripta Mater 2010;63(7):747–50.
[30] Nan ZY, Ishihara S, McEvily AJ, Shibatac H, Komano K. On the sharp bend of the S–N curve and the crack propagation behavior of extruded magnesium alloy. Scripta Mater 2007;56:649–52.
[31] Ishihara S, Nan Z, Goshima T. Effect of microstructure on fatigue behavior of AZ31 magnesium alloy. Mater Sci Eng A 2007;468–470:214–22.

Corrigendum to "Lifetime behaviour of unidirectionally wire reinforced lightweight metal matrix composites" [Int. J. Fatigue 56 (2013) 60–68]

Matthias Merzkirch *, Volker Schulze, Kay André Weidenmann

Institute for Applied Materials (IAM–WK), Karlsruhe Institute of Technology (KIT), Engelbert-Arnold-Strasse 4, 76128 Karlsruhe, Germany

The authors regret for the below correction missed:
Correction:
On pages 66 and 67, there is a wrong index
The corrected equations are:
p. 66
By using Eqs. (2) and (3), Eq. (8) can be transformed to:

$$\sigma_C = \sigma_M \cdot \left(\frac{E_{RE}}{E_M} \cdot V_{RE} + (1 - V_{RE})\right) \tag{9}$$

p. 67
By using the Basquin relation [23] for the matrix material, equation (9) can be modified as:

$$\sigma_{a,C} = \sigma'_{B,M} \cdot (N_f(M))^b \cdot \left(\frac{E_{RE}}{E_M} \cdot V_{RE} + (1 - V_{RE})\right) \tag{10}$$

The publisher would like to apologise for any inconvenience caused.

DOI of original article: http://dx.doi.org/10.1016/j.ijfatigue.2013.08.002
* Corresponding author. Tel.: +49 721 608 42753; fax: +49 721 608 48044.
E-mail address: Matthias.Merzkirch@kit.edu (M. Merzkirch).